ЖЭТФ, 2015, том 147, вып. 3, стр. 614–622

NEUTRINOS IN IceCube FROM ACTIVE GALACTIC NUCLEI

O. Kalashev [a]*, ***D. Semikoz*** [b], ***I. Tkachev*** [a]

[a] *Institute for Nuclear Research, Russian Academy of Sciences*
117312, Moscow, Russia

[b] *Laboratory of AstroParticle and Cosmology (APC)*
75205, Paris, France

Received October 27, 2014

Recently, the IceCube collaboration reported first evidence for the astrophysical neutrinos. Observation corresponds to the total astrophysical neutrino flux of the order of $3 \cdot 10^{-8}$ GeV $\cdot$ cm$^{-2} \cdot$ s$^{-1} \cdot$ sr^{-1} in a PeV energy range [1]. Active galactic nuclei (AGN) are natural candidate sources for such neutrinos. To model the neutrino creation in AGNs, we study photopion production processes on the radiation field of the Shakura–Sunyaev accretion discs in the black hole vicinity. We show that this model can explain the detected neutrino flux and at the same time avoids the existing constraints from the gamma-ray and cosmic-ray observations.

Contribution for the JETP special issue in honor of V. A. Rubakov's 60th birthday

DOI: 10.7868/S0044451015030222

1. INTRODUCTION

Detection of astrophysical neutrinos by the IceCube collaboration [1] has opened a new era in the high-energy astrophysics. The reported excess of neutrinos at energies $E > 30$ TeV can be described by a power law $1/E^{\alpha}$ with $\alpha = 2.3 \pm 0.3$, and corresponds to the flux $3 \cdot 10^{-8}$ GeV $\cdot$ cm$^{-2} \cdot$ s$^{-1} \cdot$ sr^{-1} for the sum of three flavors, possibly with a cutoff at 3 PeV [1]. This observation has a high significance of 5.7 σ and calls for theoretical modeling and explanation.

There are three main production mechanisms of high-energy neutrinos. First, galactic cosmic rays produce neutrinos in the proton–proton (proton–nucleus) collisions in the interstellar gas in the disc of our Milky Way Galaxy. Such neutrinos would have energies from sub-GeV to PeV, but can come only from directions close to the Galactic plane. Interestingly, the three-year IceCube data do show some excess in the direction of the Galactic plane with a 2 % chance probability [1], possibly exhibiting small-scale anisotropy near the Galactic center. Both signatures can be explained by the neutrino production in the galactic cosmic ray interactions with the interstellar gas. It was shown in Ref. [2] that at most 0.1 of the observed neutrino events in IceCube can be described by cosmic-ray interactions with matter inside the Milky Way assuming a local density of gas. However, the expected signal is dominated by the flux from spiral arms and/or the Galactic Bar, where supernova explosion rates, magnetic fields, and the density of the interstellar gas are all much higher than in the vicinity of the Sun [3]. Moreover, the neutrino flux detected by the IceCube is consistent [3] with the power-law extrapolation of the $E > 100$ GeV diffuse gamma-ray flux from the Galactic Ridge, as observed by the Fermi telescope, which suggests common origin. As result, the contribution of the Galaxy to the neutrino flux can be much higher than 10 %.

Second, ultra-high energy cosmic rays (UHECR) interact with intergalactic radiation and produce secondary EeV neutrinos in pion decays. The latter are called cosmogenic neutrinos and have been extensively studied theoretically since 1969 [4] (see, e. g., [5, 6] and the references therein). The expected flux of cosmogenic neutrinos is somewhat model dependent, but even optimistic estimates are at least two orders of magnitude below the IceCube signal at PeV energies. Hence, cosmogenic neutrinos are irrelevant in this energy range.

Finally, high-energy neutrinos in a wide range of energies, from TeV to 10 PeV, can be produced in a variety of astrophysical sources in decays of charged pions created in the proton–photon or proton–proton

*E-mail: kalashev@inr.ac.ru

collisions *in situ*. Various kinds of astrophysical sources of high-energy neutrinos were considered prior to the IceCube observation, including active galactic nuclei (AGN) [7–12], gamma-ray birsts [13], star burst galaxies [14].

After the IceCube observation, the interest in the problem has grown substantially. In a number of recent works [15–20], an attempt was made to explain the IceCube events by various astrophysical sources of high-energy neutrinos.

In this paper, we develop the model originally proposed in Ref. [8], where neutrinos arise in interactions of high-energy cosmic rays accelerated in AGNs with photons from the big blue bump. Compared to the previous papers developing this concept, we attempt to explain the IceCube observation using photopion production by cosmic rays on the anisotropic radiation field produced by the realistic Shakura–Sunyaev model of accretion discs [21].

This paper is organized as follows. In Sec. 2, we present theoretical details of our calculation, also reviewing the observational knowledge about black hole accretion discs and their radiation fields. In Sec. 3, we confront our numerical calculations with the IceCube result and put constraints on the properties of such prospective neutrino sources.

2. NEUTRINOS FROM AGNs WITH SHAKURA–SUNYAEV ACCRETION DISCS

AGN are long-sought potential sites for high-energy neutrino production. They can accelerate protons up to highest energies and are surrounded by high-intensity radiation fields where photo-nuclear reactions with subsequent neutrino emission can occur. At the heart of an AGN resides a super-massive black hole surrounded by the accretion disc. The accretion disc is hot and is emitting thermal radiation which gives a prominent feature in the observed AGN spectra usually referred to as the "Big Blue Bump". Accelerated particles move along two jets perpendicular to the accretion disc, crossing this radiation field.

In what follows, we use the following model for neutrino production. We assume that proton acceleration occurs directly near the black hole horizon (see, e. g., Refs. [22, 23]). High-energy neutrinos appear in charged pion decays created in $p\gamma \to n\pi^+$ and $n\gamma \to$ $\to p\pi^-$ reactions in collisions with "blue bump" photons. As a first step, we recall the observational phenomenology of accretion discs and estimate the optical depth for these photopion production reactions.

2.1. Accretion disc phenomenology

The effective temperature of the optically thick material on the scale of the gravitational radius is given by [21]

$$T_0 = 30 \text{ eV } \left(\frac{M}{10^8 M_\odot}\right)^{-1/4} \left(\frac{L}{\eta\, L_{Edd}}\right)^{1/4}, \qquad (1)$$

where M is the mass of a black hole and η is the efficiency of converting the gravitational potential energy into electromagnetic radiation, $L = \eta \dot{M}$, at a given accretion rate $\dot{M}$. The eddington luminosity L_{Edd} is defined as

$$L_{Edd} = 1.26 \cdot 10^{46} \left(\frac{M}{10^8 M_\odot}\right) \text{ erg} \cdot \text{s}^{-1}.$$

The temperature has a power-law profile with the radial coordinate on the disc, $T \propto r^{-\beta}$. In theory [21], $\beta = 3/4$. Observationally, the slope is consistent with the thin disc theory, $\beta = 0.61^{+0.21}_{-0.17}$, but would also allow a shallower temperature profile that would reduce the differences between the microlensing and flux size estimates [24].

Within uncertainties and with an accuracy sufficient for our purposes, the observed disc sizes at the radiation frequency $E_\gamma = 5$ eV can be fitted by the relation [25]

$$R = 10^{15} \text{ cm } \left(\frac{M}{10^8 M_\odot}\right),$$

which is about two orders of magnitude larger than the gravitational radius. This estimate is somewhat larger than the expectation from the thin disc theory. The photon density around the disc can be approximated by the relation

$$n_\gamma = \frac{L_{disc}}{4\pi R^2 E_c},$$

where E_c is a typical photon energy. On average, spectral energy distributions (SED) of AGNs are peaked at the energy $E_c = 10$ eV (see, e. g., Ref. [26] for a review).

The optical depth to photomeson production can be estimated as $\tau = \sigma n_\gamma R$, where $\sigma \approx 5 \cdot 10^{-28}$ cm^2 is the cross section at the Δ-resonance. This gives

$$\tau \sim 10^3 \frac{L_{disc}}{L_{Edd}} \frac{10 \text{ eV}}{E_c},$$

irrespective of the black hole mass. There are tight correlations between monochromatic and bolometric luminosities of AGNs, e. g., $\lambda L_\lambda(5100 \text{ Å}) \approx 0.1 L_{bol}$ (see [27, 28]). An estimate for L_{disc} is given by λL_λ. For a typical bolometric luminosity, we can assume

$L_{bol} \approx 0.1 L_{Edd}$ (see, e. g., Ref. [29, 30]). Therefore, $\tau \sim 10$ would be a typical value for the optical depth to photomeson production after the traveling distance comparable to the accretion disc size.

2.2. Radiation fields and reaction rates

In the laboratory frame, the rate of reactions with the photon background is given by the standard expression

$$R = \int d^3p\, n(\mathbf{p})(1-\cos\theta)\sigma(\tilde{\omega}), \tag{2}$$

where $n(\mathbf{p})$ is the photon density in the laboratory frame, $\sigma(\tilde{\omega})$ is the cross section of the relevant reaction in the rest frame of the primary particle as a function of the energy of the incident photon $\tilde{\omega} = \gamma p(1-\cos\theta)$, and γ is the gamma-factor of the primary particle in the laboratory frame.

For the black-body radiation with a temperature T, we have

$$n_T(p) \equiv \frac{2}{(2\pi)^3}\,\frac{1}{\exp(p/T)-1}. \tag{3}$$

We assume that the disc segment at a radius r emits black-body radiation with a local temperature $T(r)$,

$$T(r) = T_0\, F(r), \tag{4}$$

where T_0 is given by Eq. (1) and [21]

$$F(r) = \left(\frac{r_g}{r}\right)^{3/4}\left(1-\sqrt{\frac{r_{in}}{r}}\right)^{1/4}. \tag{5}$$

Here, $r_g = 2\kappa M$ is Schwarzschild gravitational radius,

$$r_g = 3\cdot 10^{13}\frac{M}{10^8 M_\odot}\ \text{cm},$$

and r_{in} is the radius of the disc inner edge. The contribution of such a segment to the photon density at a point z along the disc axis is

$$n(\mathbf{p}) = \frac{\delta(\mathbf{n}-\mathbf{n}_0)r\,dr}{(r^2+z^2)}\, n_T(p,r), \tag{6}$$

where $\mathbf{n}_0$ is the unit vector in the direction from r to z. Its contribution to the reaction rate in Eq. (2) can be expressed as

$$R(z,r,\gamma) = \frac{1-\cos\theta}{4\pi^3(r^2+z^2)}\int\limits_0^\infty \frac{dp\,p^2\,\sigma(\tilde{\omega})}{\exp(p/T(r))-1}, \tag{7}$$

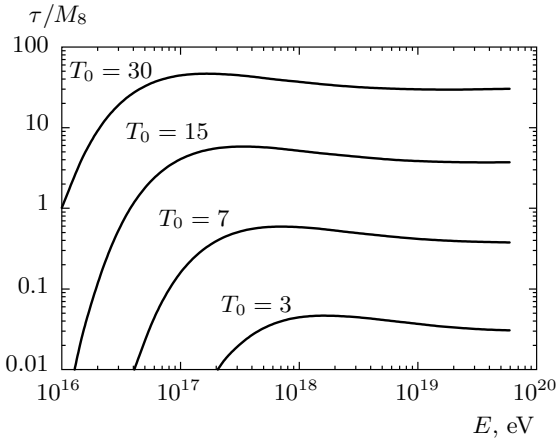

Fig. 1. Optical depth as a function of the proton energy for several values of T_0 (in eV)

where $\cos\theta = z/\sqrt{r^2+z^2}$. Finally,

$$R(z,\gamma) = 2\pi\int\limits_{r_{in}}^\infty r\,dr R(z,r,\gamma). \tag{8}$$

The disc inner edge r_{in} is related to the radiation efficiency as

$$\eta = \frac{3}{2}\int\limits_{r_{in}}^\infty r\,dr\,F^4(r).$$

In what follows, we use $\eta = 0.1$, which is a usual assumption in the existing literature.

The optical depth with respect to this reaction for protons accelerated near the black hole horizon and moving along the jet axis from z_0 to infinity is given by

$$\tau(\gamma) = \int\limits_{z_0}^\infty dz\, R(z,\gamma).$$

The resulting function $\tau(E)$ for photomeson production is shown in Fig. 1 for several values of T_0[1)] and $z_0 = r_g$. To produce neutrinos with the energy $E_\nu \sim 10^{15}$ eV efficiently, we need the optical depth with respect to this reaction to be larger than unity for protons with $E \sim 10^{17}$ eV. This requirement translates into $T_0 > 10$ eV (see Fig. 1).

3. THE OBSERVED SPECTRUM

In this paper, we do not study the processes of particle acceleration but simply assume that protons are

[1)] We note that the average background photon energy is roughly $0.1T_0$.

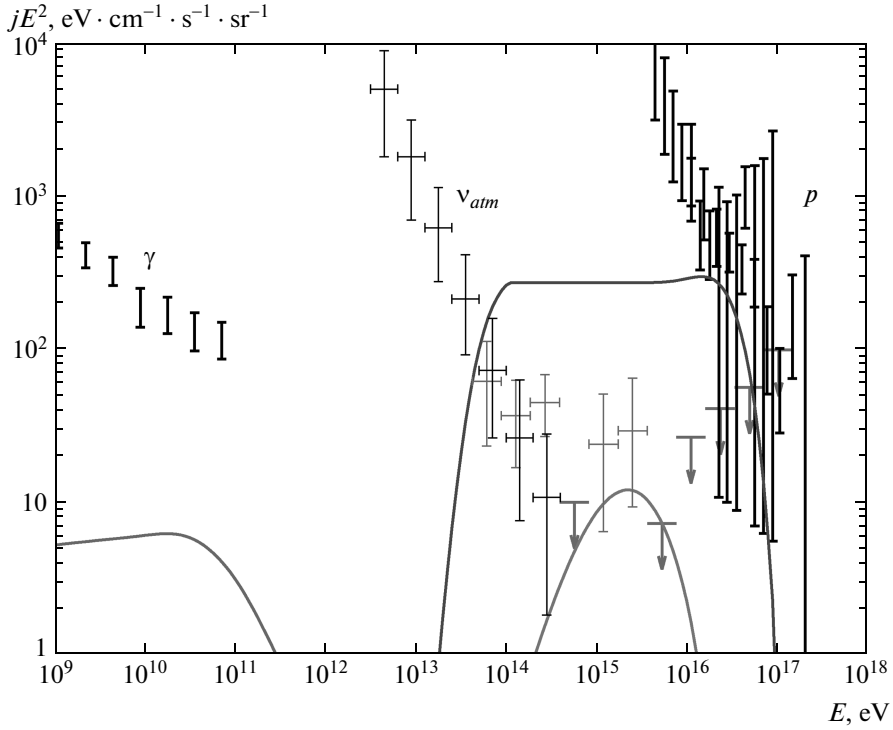

Fig. 2. Secondary neutrino (red line) and gamma-ray (magenta line) fluxes from protons (blue line) with the $1/E^2$ power-law injection spectrum and $E_{max} = 100$ PeV for the disc temperature $T_0 = 15$ eV, the black hole mass $10^8 M_\odot$, and the luminosity evolution of sources $(1+z)^3$. Red points with errorbars represent the IceCube astrophysical neutrino flux from Ref. [1]. The atmospheric neutrino flux is taken from Ref. [34], the Fermi diffuse gamma-ray flux is from Ref. [35], and the proton flux is from Ref. [36]. (Color online see arXiv:1410.8124)

accelerated by electric fields in a close vicinity of the black hole horizon (see, e. g., Ref. [22] for relevant models). For definiteness, we assume that the spectrum of accelerated protons at $z = z_0$ has the power-law form

$$j_{acc}(E) = E^{-\alpha}, \quad E < E_{max}, \tag{9}$$

their momenta are directed along the disc axis, and electric fields and acceleration proceses are negligible at larger z. In what follows, we choose $\alpha = 2$ and $z_0 = 2r_g$.

The calculation of the observable neutrino spectrum is performed in two steps. First, we simulate propagation of protons through the radiation field at $z > z_0$ and calculate the resulting spectrum of nucleons and of products of their interaction. To be conservative, we assume that the magnetic field is negligible and therefore both protons and neutrons with energies below the pion production threshold may freely escape the source. This allows calculating the maximal possible contribution of the process to the observed spectrum of cosmic rays. As regards the secondary electron–photon cascade calculation, to obtain its upper bound, we always assume that the cascade freely escapes the source region and show below that even in this extreme case, the predicted contribution of this process to the diffuse photon background is far below the present observational upper limits.

We model interactions using the Monte Carlo approach. In particular, during the ith iteration at a position $z = z_i$, the traveled optical depth τ_i is sampled using the equation

$$\tau_i = -\log \xi.$$

Here and below, ξ is a uniformly distributed random variable, $0 < \xi < 1$. The next interaction point z_{i+1} is calculated by solving the equation

$$\int_{z_i}^{z_{i+1}} R(z, \gamma_i)\, dz = \tau_i, \tag{10}$$

where γ_i is the current gamma factor of the nucleon and $R(z, \gamma_i)$ is the interaction rate given by Eq. (8). The background photon momentum is sampled in each

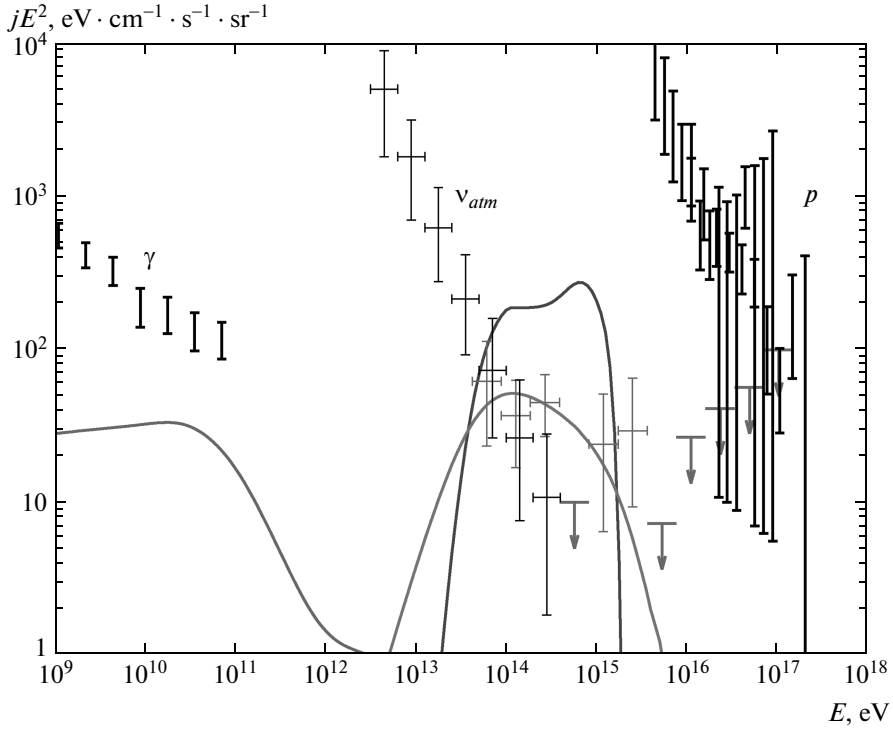

Fig. 3. Secondary neutrino and gamma-ray fluxes from protons with the $1/E^2$ power-law spectrum and $E_{max} = 30$ PeV for $T_0 = 120$ eV and the luminosity evolution of sources proportional to $(1+z)^3$. Experimental data are the same as in Fig. 2. (Color online see arXiv:1410.8124)

interaction point z_i in the following way. First, the disc segment r_i emitting the photon is sampled using Eq. (8):

$$\xi R(z,\gamma) = 2\pi \int\limits_{r_{in}}^{r_i} r\,dr\,R(z_i,r,\gamma), \qquad (11)$$

and then the photon energy p_i is sampled using Eq. (7):

$$\xi R(z,r,\gamma) = \frac{1-\cos\theta_i}{4\pi^3(r_i^2+z_i^2)} \int\limits_0^{p_i} \frac{dp\,p^2\,\sigma(\tilde{\omega})}{\exp(p/T(r_i))-1}, \qquad (12)$$

where $\cos\theta_i = z_i/\sqrt{z_i^2+r_i^2}$. Finally, the SOPHIA event generator [31] is used to sample the recoiling nucleon energy γ_{i+1} as well as secondary particles and their momenta. The iterations continue while Eq. (10) has a solution. The absence of solutions means that the nucleon freely escapes the AGN site. As a result, we obtain the spectrum of nucleons, neutrinos, photons, and electrons leaving the interaction region.

In the second step, we integrate over the distribution of sources taking their possible abundance evolution and cosmological propagation effects into account[2)]. The last effect mostly reduces to red shift, neutron decay, and electron–photon cascade development led by interactions with the cosmic microwave background and intergalactic infrared background. This procedure is performed with the use of the numerical code developed in Ref. [32]. The code simulates interactions of nucleons, photons, and stable leptons with intergalactic photon backgrounds. For nucleons, it takes photopion production, e^+e^--pair production, and neutron decay into account. The secondary particles produced in these interactions are also traced in the code. The electron–photon cascade is mostly driven by the chain of inverse Compton scattering of electrons on background photons and e^+e^--pair production by photons. We also take neutrino mixing into account using the mixing angles in the tribimaximal approximation, which is sufficient with the current limited statistics. The resulting spectrum has a flavor ratio of approximately (1:1:1).

Finally, we normalize the simulated spectra using the IceCube data. Namely, using 22 events with the deposited energy above 42 TeV, published in Ref. [1],

[2)] We do not average over T_0 and E_{max}.

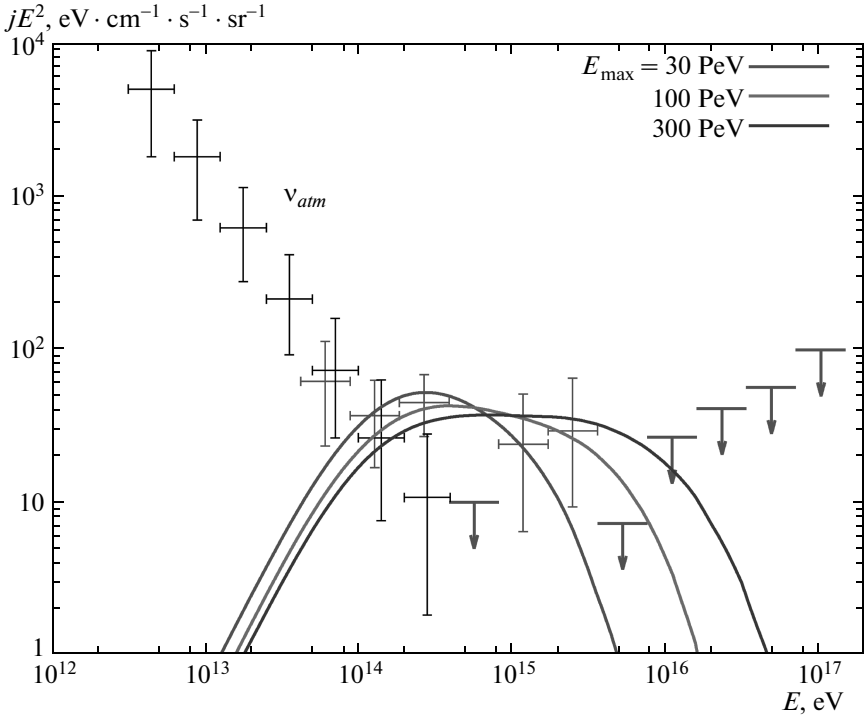

Fig. 4. Dependence of the neutrino flux on maximum proton energy E_{max} for E^{-2} power-law injection spectrum, the disc temperature $T_0 = 60$ eV and the luminosity evolution of sources $\propto (1+z)^3$. Red points with errorbars show the IceCube astrophysical neutrino flux after 3 years of exposure, taken from Ref. [1]. The atmospheric neutrino flux, Ref. [34], is shown by black points with errorbars. (Color online see arXiv:1410.8124)

and the exposure dependence on energy from Ref. [33], we maximize the Poisson probability of observing the above events under the condition that a given theoretical model is true.

In the energy bin 0.4–1 PeV, the IceCube does not have any events in the present data. According to Ref. [1], a gap larger than this one appears in 43 % of realizations of the best-fit continuous spectra. Therefore, we can safely assume that the real neutrino spectrum is described by a smooth power law. On the other hand, different energy regions may correspond to different populations of sources, and therefore the spectrum may have features. For example, a peak at $E_\nu \sim 2$ PeV might be real. Presently both possibilities should be considered, and we follow this line of thought in presenting the results.

In Fig. 2, we present the secondary neutrino flux (shown in red) from protons accelerated to $E_{max} = 100$ PeV and absorbed in the disc radiation field with the temperature $T_0 = 15$ eV (the black hole mass $10^8 M_\odot$ and luminosity evolution of sources $(1+z)^3$ is assumed). We see that the resulting neutrino spectrum is rather narrow[3)], and therefore the population of objects with such a low temperature may explain narrow bumps in the spectrum.

Figure 3 corresponds to $T_0 = 120$ eV and $E_{max} = 30$ PeV. In this, case all high-energy part of the IceCube neutrino flux at $E > 100$ TeV can be explained assuming that the absence of events in the energy bin 0.5–1 PeV is due to a statistical fluctuation. One would have to explain low-energy data $E < 100$ TeV with other type of sources still, if such data will appear, because our model has a low-energy cutoff at 100 TeV due to the energy threshold for photopion production.

The calculated secondary photon flux in all cases is significantly below the diffuse γ-background measured by Fermi. The measured [36] proton flux at energies $E = 1$–100 EeV is dominated by Galactic sources (see, e. g., Ref. [37]). Therefore, the contribution of extragalactic sources to the observed proton flux should be

[3)] We have studied the models with monochromatic injection spectra of accelerated protons as well. The resulting neutrino spectra are somewhat narrower, compared to a power law injection, but are not monochromatic.

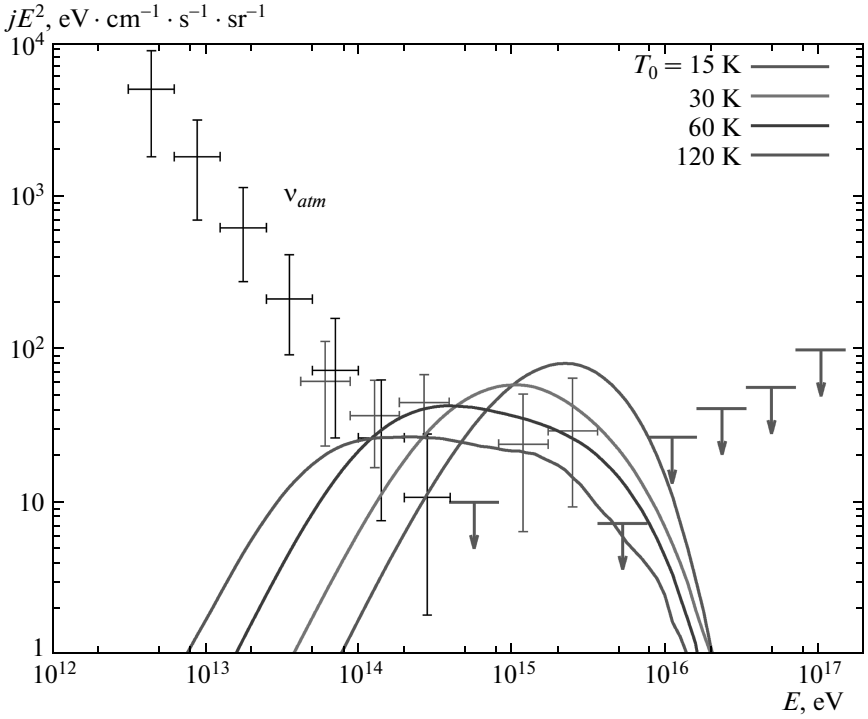

Fig. 5. Dependence of the neutrino flux on the disc temperature T_0 for $E_{max} = 100$ PeV. The remaining parameters and experimental data are the same as in Fig. 4. (Color online see arXiv:1410.8124)

subdominant. Our results do not contradict this observation either.

The model dependence of the resulting neutrino flux is shown in Figs. 4, 5. In Fig. 4, the dependence on the maximum energy of accelerated protons is presented for $T_0 = 60$ eV. Models with the maximum energies $E_{max} = 30$ PeV, $E_{max} = 100$ PeV, and $E_{max} = 300$ PeV are shown with red, green, and blue lines. In Fig. 5, we present the dependence of the neutrino flux on the disc temperature for $E_{max} = 100$ PeV. Disc temperatures $T_0 = 15$ eV, $T_0 = 30$ eV, $T_0 = 60$ eV, and $T_0 = 120$ eV are respectively shown with red, green, blue, and pink lines. The spectrum of neutrinos for $T_0 = 15$ eV is peaked at 1–3 PeV and may be responsible for the high-energy part of the IceCube data. The case of the high temperature $T_0 = 120$ eV can explain the IceCube data for the whole energy range $E > 100$ TeV.

4. DISCUSSION

We have made an attempt to explain the extragalactic neutrino signal recently announced by the IceCube collaboration [1]. As the prospective class of neutrino sources, we have chosen AGNs. To model neutrino creation, we study photopion production processes on the radiation field of the Shakura–Sunyaev accretion discs in the black hole vicinity. To our knowledge, our work is the first where a realistic anisotropic radiation field of the accretion disc is considered for these purposes.

Important parameters describing the model are the maximum energy of accelerated protons and the disc temperature. We have studied the parameter space of the model and compared the predicted neutrino fluxes with the IceCube measurement. Along the way we took into account the constraints set by the diffuse gamma-ray background measurements by the Fermi observatory [35] and by the proton flux measurements by KASCADE and KASCADe-Grande experiments [36]. We have shown that the model presented in this paper can naturally explain the neutrino spectrum observed by the IceCube. The model can be falsified (and better constrained) by studying the correlation signal between neutrino arrival directions and varios subclasses of AGNs. Such study will became feasible in the nearest future, as more data are accumulated. Current strong directional bounds on the possible neutrino sources are given, e. g., in Ref. [38, 39].

This work was supported by the Russian Science Foundation, grant 14-12-01340. Numerical calculations were performed at the computer cluster of the Theoretical Physics Division of the Institute for Nuclear Research, Russian Academy of Sciences.

REFERENCES

1. M. G. Aartsen et al. [IceCube Collaboration], Phys. Rev. Lett. **113**, 101101 (2014); arXiv:1405.5303 [astro-ph.HE].
2. J. C. Joshi, W. Winter, and N. Gupta, arXiv:1310.5123 [astro-ph.HE].
3. A. Neronov, D. V. Semikoz, and C. Tchernin, Phys. Rev. D **89**, 103002 (2014); arXiv:1307.2158 [astro-ph.HE].
4. V. S. Berezinsky and G. T. Zatsepin, Phys. Lett. **28** B, 423 (1969).
5. O. E. Kalashev, V. A. Kuzmin, D. V. Semikoz, and G. Sigl, Phys. Rev. D **66**, 063004 (2002); arXiv: hep-ph/0205050.
6. D. V. Semikoz and G. Sigl, JCAP **0404**, 003 (2004); arXiv:hep-ph/0309328.
7. D. Eichler, Astrophys. J. **232**, 106 (1979).
8. F. W. Stecker, C. Done, M. H. Salamon, and P. Sommers, Phys. Rev. Lett. **66**, 2697 (1991); Erratum-ibid. **69**, 2738 (1992).
9. A. Atoyan and C. D. Dermer, Phys. Rev. Lett. **87**, 221102 (2001); arXiv:astro-ph/0108053.
10. F. Halzen and E. Zas, Astrophys. J. **488**, 669 (1997).
11. A. Y. Neronov and D. V. Semikoz, Phys. Rev. D **66**, 123003 (2002); arXiv:hep-ph/0208248.
12. M. Kachelriess, S. Ostapchenko, and R. Tomas, New J. Phys. **11**, 065017 (2009); arXiv:0805.2608 [astro-ph].
13. E. Waxman and J. N. Bahcall, Phys. Rev. Lett. **78**, 2292 (1997); arXiv:astro-ph/9701231.
14. A. Loeb and E. Waxman, JCAP **0605**, 003 (2006); arXiv:astro-ph/0601695.
15. I. Cholis and D. Hooper, JCAP **1306**, 030 (2013); arXiv:1211.1974 [astro-ph.HE].
16. F. W. Stecker, Phys. Rev. D **88**, 047301 (2013); arXiv:1305.7404 [astro-ph.HE].
17. K. Murase and K. Ioka, Phys. Rev. Lett. **111**, 121102 (2013); arXiv:1306.2274 [astro-ph.HE].
18. L. A. Anchordoqui, V. Barger, I. Cholis, H. Goldberg, D. Hooper, A. Kusenko, J. G. Learned, and D. Marfatia, JHEAp **1–2**, 1 (2014); arXiv:1312.6587 [astro-ph.HE].
19. C. D. Dermer, K. Murase, and Y. Inoue, JHEAp **3–4**, 29 (2014); arXiv:1406.2633 [astro-ph.HE].
20. K. Murase, Y. Inoue, and C. D. Dermer, Phys. Rev. D **90**, 023007 (2014); arXiv:1403.4089 [astro-ph.HE].
21. N. I. Shakura and R. A. Sunyaev, Astron. Astrophys. **24**, 337 (1973).
22. A. Y. Neronov, D. V. Semikoz, and I. I. Tkachev, New J. Phys. **11**, 065015 (2009); arXiv:0712.1737 [astro-ph].
23. O. E. Kalashev, K. V. Ptitsyna, and S. V. Troitsky, Phys. Rev. D **86**, 063005 (2012); arXiv:1207.2859 [astro-ph.HE].
24. C. W. Morgan, C. S. Kochanek, N. D. Morgan, and E. E. Falco, arXiv:0707.0305 [astro-ph].
25. C. W. Morgan, C. S. Kochanek, N. D. Morgan, and E. E. Falco, Astrophys. J. **712**, 1129 (2010); arXiv: 1002.4160 [astro-ph.CO].
26. A. Koratkar and O. Blaes, PASP **111**, 1 (1999).
27. M. Elvis, B. J. Wilkes, J. C. McDowell, R. F. Green, J. Bechtold, S. P. Willner, M. S. Oey, and E. Polomski, Astrophys. J. Suppl. **95**, 1 (1994).
28. G. T. Richards, M. Lacy, L. J. Storrie-Lombardi, P. B. Hall, S. C. Gallagher, D. C. Hines, X. Fan, and C. Papovich, Astrophys. J. Suppl. **166**, 470 (2006); arXiv:astro-ph/0601558.
29. J. -H. Woo and C. M. Urry, Astrophys. J. **579**, 530 (2002); arXiv:astro-ph/0207249.
30. S. Kaspi, P. S. Smith, H. Netzer, D. Maoz, B. T. Jannuzi, and U. Giveon, Astrophys. J. **533**, 631 (2000); arXiv:astro-ph/9911476.
31. A. Mucke, R. Engel, J. P. Rachen, R. J. Protheroe, and T. Stanev, Comput. Phys. Comm. **124**, 290 (2000); arXiv:astro-ph/9903478.
32. O. E. Kalashev, V. A. Kuzmin, and D. V. Semikoz, arXiv:astro-ph/9911035; Mod. Phys. Lett. A **16**, 2505 (2001); arXiv:astro-ph/0006349; O. E. Kalashev, Ph. D. Thesis, INR RAS (2003); O. E. Kalashev and E. Kido, arXiv:1406.0735 [astro-ph.HE].
33. L. A. Anchordoqui, H. Goldberg, M. H. Lynch, A. V. Olinto, T. C. Paul, and T. J. Weiler, Phys. Rev. D **89**, 083003 (2014); arXiv:1306.5021 [astro-ph.HE].

34. R. Abbasi et al. [IceCube Collaboration], arXiv: 1104.5187 [astro-ph.HE].

35. A. A. Abdo et al. [The Fermi-LAT collaboration], Phys. Rev. Lett. **104**, 101101 (2010); arXiv:1002.3603 [astro-ph.HE].

36. W. D. Apel et al. [KASCADE-Grande Collaboration], Astropart. Phys. **47**, 54 (2011).

37. G. Giacinti, M. Kachelriess, and D. V. Semikoz, Phys. Rev. D **90**, 041302 (2014); arXiv:1403.3380 [astro-ph.HE].

38. S. Adrian-Martinez et al. [ANTARES Collaboration], Astrophys. J. **786**, L5 (2014); arXiv:1402.6182 [hep-ex].

39. M. G. Aartsen et al. [IceCube Collaboration], arXiv: 1406.6757 [astro-ph.HE].